JOURNAL OF VIROLOGY, June 2007, p. 5637–5648 Vol. 81, No. 11
0022-538X/07/$08.00+0 doi:10.1128/JVI.02360-06


# Antiviral Effects of Antisense Morpholino Oligomers in Murine Coronavirus Infection Models[▽]

Renaud Burrer,[1]† Benjamin W. Neuman,[1]‡ Joey P. C. Ting,[1] David A. Stein,[3] Hong M. Moulton,[3] Patrick L. Iversen,[3] Peter Kuhn,[2] and Michael J. Buchmeier[1]*

*Department of Molecular and Integrative Neurosciences[1] and Department of Cell Biology,[2] The Scripps Research Institute, 10550 North Torrey Pines Rd., La Jolla, California 92037, and AVI Biopharma Inc., 4575 SW Research Way, Corvallis, Oregon 97333[3]*

Received 27 October 2006/Accepted 1 March 2007

**The recent emergence of novel pathogenic human and animal coronaviruses has highlighted the need for antiviral therapies that are effective against a spectrum of these viruses. We have used several strains of murine hepatitis virus (MHV) in cell culture and in vivo in mouse models to investigate the antiviral characteristics of peptide-conjugated antisense phosphorodiamidate morpholino oligomers (P-PMOs). Ten P-PMOs directed against various target sites in the viral genome were tested in cell culture, and one of these (5TERM), which was complementary to the 5′ terminus of the genomic RNA, was effective against six strains of MHV. Further studies were carried out with various arginine-rich peptides conjugated to the 5TERM PMO sequence in order to evaluate efficacy and toxicity and thereby select candidates for in vivo testing. In uninfected mice, prolonged P-PMO treatment did not result in weight loss or detectable histopathologic changes. 5TERM P-PMO treatment reduced viral titers in target organs and protected mice against virus-induced tissue damage. Prophylactic 5TERM P-PMO treatment decreased the amount of weight loss associated with infection under most experimental conditions. Treatment also prolonged survival in two lethal challenge models. In some cases of high-dose viral inoculation followed by delayed treatment, 5TERM P-PMO treatment was not protective and increased morbidity in the treated group, suggesting that P-PMO may cause toxic effects in diseased mice that were not apparent in the uninfected animals. However, the strong antiviral effect observed suggests that with further development, P-PMO may provide an effective therapeutic approach against a broad range of coronavirus infections.**

In 2002–2003, the severe acute respiratory syndrome (SARS) outbreak resulted in over 8,000 cases and more than 770 fatalities worldwide and focused attention on the potential pathogenicity of human coronaviruses. The responsible agent, SARS coronavirus (SARS-CoV), was transmitted to humans from its bat reservoir (17) by an intermediate host, the palm civet, and possibly other animal vectors (9). Once established in humans, the infection spread directly from person to person by aerosol or droplets. Although the future reemergence of SARS-CoV remains possible, the virus has not reappeared since the last documented case in 2003, except for sporadic (18) or lab-related (26) cases. However, two other new human coronaviruses, namely, CoV-NL63 (33), a group 1 coronavirus associated with bronchiolitis and lower respiratory tract infections, and CoV-HKU1 (35), a group 2 coronavirus associated with pneumonia, have been identified in the interval, and the previously known human coronaviruses 229E and OC43 continue to circulate. The development of antiviral drugs that could be used to treat coronavirus-infected patients thus remains of significant importance to public health.

Murine hepatitis virus (MHV) is a close phylogenetic relative of SARS-CoV; both are currently classified within the group 2 coronaviruses (8). Depending on the route of infection, different MHV strains can be used as disease models for hepatitis, encephalomyelitis, gastrointestinal infection, and upper respiratory disease in mice. MHV-A59, MHV-2, and MHV-3 injected intraperitoneally (i.p.) provoke hepatitis (1, 22). Intranasal (i.n.) or intracranial injection of neurotropic strains, including MHV-A59 and MHV-4 (JHM), results in acute encephalitis followed by a demyelinating disease that resembles multiple sclerosis in some surviving mice (14). MHV-1 was recently reported to replicate in the lungs of several mouse strains after i.n. inoculation, producing an upper respiratory syndrome that resembles SARS-CoV infection in humans (40).

Phosphorodiamidate morpholino oligomers (PMOs) are single-stranded DNA-like compounds that bind to mRNA by Watson-Crick base pairing and can inhibit gene expression by steric blockade of cRNA (31). PMOs have been used widely for several years to specifically interfere with the expression of cellular genes (11). Conjugation of various arginine-rich peptides to PMOs has routinely been used to increase PMO uptake into mammalian cells and offers the additional advantage of increased antisense efficacy once duplexed with target RNA compared to that of nonconjugated PMOs (23). Several recent studies have also demonstrated the potential of PMO and

* Corresponding author. Mailing address: The Scripps Research Institute, Department of Molecular and Integrative Neurosciences, Mail Drop SP30-2020, 10550 N. Torrey Pines Rd., La Jolla, CA 92037. Phone: (858) 784-7164. Fax: (858) 784-7369. E-mail: buchm@scripps.edu.

† Present address: Centre d'Immunologie de Marseille-Luminy, Marseille, France.

‡ Present address: University of Reading, Reading, Berkshire, United Kingdom.

▽ Published ahead of print on 7 March 2007.

TABLE 1. P-PMO sequences and target sites

| P-PMO name | Sequence (5′–3′) | Target site (nt positions) |
|---|---|---|
| 5TERM | CGGACGCCAATCACTCTTATA | Genomic 5′ terminus (2–22)[a] |
| (+)19-40 | GAGTTGAGAGGGTACGTACGGA | Genomic leader stem-loop 1 (19–40) |
| TRS1 | GTTTAGATTAGATTTAAACTAC | Genomic and subgenomic TRS region (51–72) |
| TRS2 | CGTTTATAAAGTTTATATTAGAT | Genomic TRS region (60–82) |
| 5UTR | TGACAAGACCAGGCCCGCGG | Genomic region between leader and pp1ab AUG (104–123) |
| AUG | TCTTTGCCATTATGCAACCTA | Genomic pp1ab AUG region (200–220) |
| 1ABFS | GACGGGCATTTACACTTGTAC | Genomic pp1ab ribosomal frameshift signal (13612–13632) |
| MBTRS | GTACTACTCATAATGTTTAGAT | Sub genomic RNA 6 TRS region (28958–28979) |
| (−)3TERM | TATAAGAGTGATTGGCGTCCG | Antigenomic 3′ terminus (2–22)[b] |
| (−)19-40 | TCCGTACGTACCCTCTCAACTC | Antigenomic leader stem-loop 1 (18–39)[b] |
| RND | AGTCTCGACTTGCTACCTCA | Randomized control sequence |
| SARS-TRS1 | GTTCGTTTAGAGAACAGATC | SARS-CoV genomic leader TRS region (53–72)[c] |
| SARS-5TERM | GGTAGGTAAAAACCTAATAT | SARS-CoV genomic 5′ terminus (1–20) |

[a] MHV nucleotide positions based on GenBank sequence accession no. AY700211.
[b] Positions of the complementary genomic nucleotide positions are specified.
[c] SARS-CoV positions based on GenBank accession no. AY274119.

peptide-PMO (P-PMO) compounds as antiviral agents, with activity against several flaviviruses (4, 12, 13), arteriviruses (32, 39), and influenza virus (7) in cell culture and against Ebola virus (6, 34) and coxsackievirus B3 (38) both in cell culture and in vivo.

Our laboratory has previously reported that antisense P-PMOs can inhibit coronavirus replication in cell culture. P-PMOs complementary to the genomic RNA of MHV (25) or SARS-CoV (24) were shown to be effective, with 50% inhibitory concentrations in the low micromolar range. In the present study, we extend these previous findings and report the investigation of the effects of PMO compounds on MHV replication and disease in vivo. We evaluated 10 MHV P-PMOs in cell culture experiments and found that one, with a sequence complementary to the 5′-terminal sequence of the viral genome (5TERM), consistently generated the highest level of specific inhibition against each MHV strain challenged. In vivo, 5TERM P-PMO decreased viral replication in the livers of animals infected with various strains of MHV. Histologic examination revealed that the reduction in the severity of liver tissue damage corresponded with a decreased viral load. Prophylactic treatment with 5TERM P-PMO resulted in an improved clinical status of animals after i.p. challenge with each of three strains of MHV at all inoculum doses tested. However, morbidity and mortality, paradoxically, increased when administration of P-PMO treatment was delayed until 1 day after infection with high doses of MHV-Alb139. Similar results were obtained with MHV-1 in the lung, where certain antiviral and ineffective P-PMO regimens aggravated clinical disease compared to that in infected controls, irrespective of the level of viral replication. These results collectively reveal both the antiviral activity and potential toxicity of P-PMO treatment in therapeutically relevant MHV challenge models.

## MATERIALS AND METHODS

**Cells and viruses.** DBT and Vero-E6 cells were cultured in Dulbecco's modified Eagle's medium containing 10% fetal bovine serum, 0.01 M HEPES, penicillin, and streptomycin for general growth and maintenance and in serum-free medium (VP-SFM; Invitrogen) supplemented with L-glutamine and antibiotics during P-PMO studies. MHV-1 was obtained from ATCC. MHV-2, MHV-3, MHV-4 (JHM), and MHV-A59 were obtained from previously described sources (27). Alb139 (5, 19) was obtained from P. Rottier. MHV stocks were produced on 17Cl-1 cells (MHV-1) or DBT cells (all other strains), and titers were determined by plaque assay as previously described (25). SARS-CoV-Tor2 was cultivated on Vero-E6 cells as previously described (24).

**PMO and P-PMO design and synthesis.** PMOs (30), P-PMOs with a thioether linker (20, 21, 23), and P-PMOs with an amide linker (2) were produced at AVI Biopharma Inc. (Corvallis, OR) by previously described methods. PMO sequences and target locations in MHV or SARS-CoV are specified in Table 1 and represented schematically in Fig. 1A. Previous studies with SARS-CoV (24) and equine arteritis virus (32) demonstrated that P-PMOs targeting conserved sequence elements of the genomic 5′-untranslated region (5′-UTR) reduced viral replication. Therefore, several PMOs were designed against the sequence in the 5′-UTR of MHV or SARS-CoV (the first six and last two entries in Table 1, respectively) to potentially interfere with translation of the viral replicase polyprotein, pp1ab. A previous study (24) also demonstrated that a P-PMO complementary to the ribosomal frameshift signal between the 1a and 1b open reading frames inhibited SARS-CoV replication, and therefore a PMO was designed to interrupt ribosomal frameshifting of MHV (1ABFS). Another PMO (MBTRS) was designed complementary to the body transcription regulatory sequence (TRS) region of RNA, coding for the structural protein M, to potentially interfere with discontinuous synthesis of the subgenomic RNA containing the M coding sequence. PMOs were also designed to duplex with the 3′ termini of (−)-sense genomic and subgenomic viral RNAs [(−)3TERM and (−)19-40, respectively].

Several arginine-rich cell-penetrating peptides (CPPs) were prepared, conjugated to PMOs, and evaluated for functional efficiency. In an initial screening, all PMOs were conjugated with the oligoarginine peptide $R_9F_2$. The CPP $(RXR)_4XB$ (X = 6-aminohexanoic acid; B = beta-alanine) has been reported to be more stable (23, 37), and less toxic (2, 7), than $R_9F_2$. Therefore, subsequent experiments utilized a panel of CPPs having two to four repeats of the RXR peptide motif conjugated to a PMO through one of two linkers, either a thioether bond between the HS group of the cysteine (C) and the PMO or an amide bond between the carboxyl group of beta-alanine and the PMO. The series of peptide-linker compositions was designed to investigate the effects of RXR repeat number and linker makeup on the ability to deliver PMOs into cells and to determine the relative toxicities of the various conjugates.

It has been shown that liver uptake of peptide nucleic acids (PNA) (10) and a triplex-forming oligonucleotide (TFO) (36) is enhanced by glycosylation. Therefore, two mannosylated conjugates, Man-$(RXR)_4$XB-5TERM and Man-$(RX)_4$C-5TERM, in addition to the corresponding nonmannosylated conjugates, were evaluated both in cell culture and in mice to determine the effect of the carbohydrate modification on the activities of both P-PMOs. The mannose-modified P-PMO conjugates were synthesized as described below. Three acetyl-protected and 9-fluorenylmethoxy carbonyl-modified mannosyl serine residues (Sussex, Ottawa, Ontario, Canada) were sequentially appended to the N terminus of the $(RX)_4$B or $(RXR)_4$XB peptide, using standard 9-fluorenylmethoxy carbonyl chemistry. Using a previously described method (2), the acetyl-protected mannose-modified peptides were conjugated to PMOs, and the conjugates were purified. Removal of acetyl protection groups from the mannoses of a conjugate was carried out by dissolving the conjugate in a dimethyl sulfoxide-methanol (1/1 [vol/vol]) solution (700 μM), followed by incremental addition of

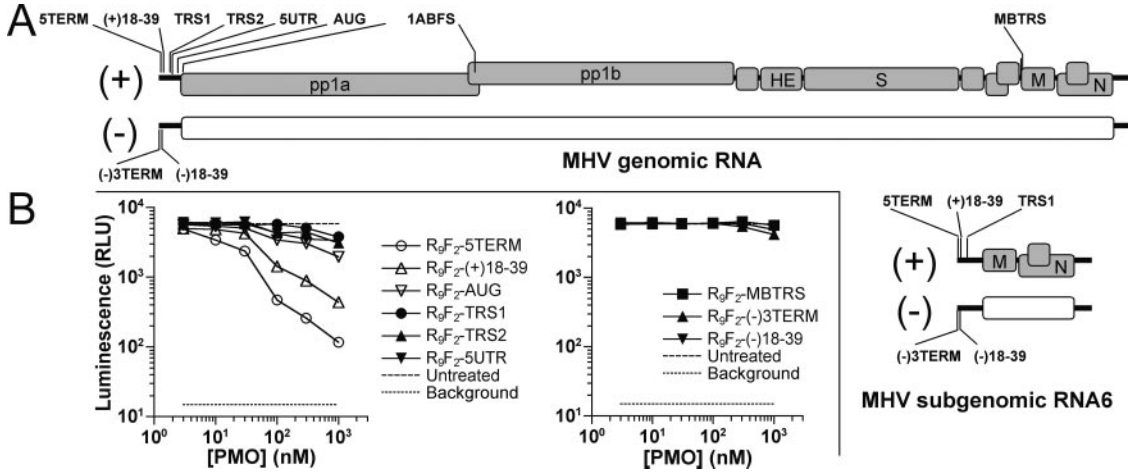


FIG. 1. P-PMO target sites and efficacy evaluation in a reporter assay. (A) Locations targeted by each PMO compound on the genomic (+) and antigenomic (−) viral RNA (top) and on the subgenomic RNAs (lower right; example given is RNA6). (B) Comparison of translation inhibitory activities by P-PMOs against in vitro-transcribed RNA consisting of the MHV 5′-UTR sequence fused to luciferase in rabbit reticulocyte lysate in vitro translation reactions. Activities of P-PMOs complementary to the genomic MHV 5′-UTR (left) and other regions of viral RNA (right) from the same experiment are depicted. Error bars indicate standard errors of the means.

0.2 M $CH_3ONa$ (in $CH_3OH$) to bring the pH of the solution to 11.5 to 12.5. The mannosyl $(RX)_4$-PMO and $(RXR)_4$-PMO solutions were stirred at room temperature for 2 and 1 h, respectively. The solutions were neutralized with 0.2 M $CH_3COOH$ and purified by cationic-exchange and reverse-phase chromatography as described elsewhere (21). The mass of each mannosylated P-PMO was confirmed by matrix-assisted laser desorption ionization–time-of-flight mass spectrometry, and purities were about 85%, as analyzed by high-pressure liquid chromatography.

**Cell-free translation assays.** The protein coding sequence for firefly luciferase, without the translation initiator Met codon, was subcloned into the multiple cloning site of plasmid pCiNeo (Promega) at the SalI and NotI sites. Subsequently, complementary oligonucleotides carrying the complete MHV-A59 (GenBank accession no. NC_001846) 5′-UTR and the first 42 nucleotides (nt) of coding sequence were duplexed and subcloned into the NheI and SalI sites, creating pM5′luc. RNAs were transcribed in vitro, and cell-free translation inhibition assays were carried out with rabbit reticulocyte lysate as previously described (25).

**Virus multiplication assay.** DBT or Vero-E6 cells were seeded at a density of $5 \times 10^5$ cells per 25-$cm^2$ tissue culture flask and allowed to adhere overnight at 37°C with 5% $CO_2$. Cells were incubated for at least 3 h with 1 ml VP-SFM containing the specified treatment. After removal of treatment-containing medium, cells were inoculated with MHV or SARS-CoV and placed at 37°C for 1 h. The inoculum was removed and replaced with fresh treatment-containing VP-SFM as specified.

**Plaque assay.** For titration of infectious virus, DBT cells (for MHV) or Vero-E6 cells (for SARS-CoV) were seeded in 12-well tissue culture plates at $2 \times 10^5$ cells per well and allowed to adhere overnight at 37°C with 5% $CO_2$. The culture medium was removed and replaced with 0.5 ml of cell culture supernatant or tissue homogenate from viral experiments. A 0.7% agarose overlay containing 2% fetal bovine serum was applied to cells 1 h after inoculation. After 72 h, cells were fixed by immersion in 10% formaldehyde in phosphate-buffered saline (PBS) for 24 h, agarose plugs were removed, and cells were stained with 0.1% crystal violet. Plaque size reduction assays were performed with untreated cells that were inoculated with fixed doses of MHV and, after 1 h, treated with P-PMO as previously described (24). A single dose of P-PMO was applied together with the agarose overlay. Plaque diameters were measured with a ruler to the nearest 0.5 mm.

**Resistance studies.** Plaque-purified MHV-A59 was passaged 10 times on fresh DBT cells subjected to treatment with 10 μM P-PMO for 4 h before each infection period. Twenty-four hours after inoculation, the cell culture medium was removed and either aliquoted for plaque assay titration or used to initiate the subsequent round of infection of P-PMO-treated cells.

**Infections and treatment in mouse models.** Five-week-old male C57BL/6 mice were obtained from The Scripps Research Institute's breeding facility. Viruses were diluted in saline and injected either i.p. in a total volume of 250 μl for the hepatitis models or i.n. in 20 μl saline for the respiratory infection model. For each experiment, PMOs/P-PMOs were diluted in 0.9% saline and injected i.p., except where specified. For viral growth and histopathology experiments, where mice were sacrificed at day 4 postinfection (p.i.), each mouse received one dose (20 nanomoles of nonconjugated PMO or 8 nanomoles of P-PMO) 5 h before and 24 h and 48 h after infection, for a total of three doses per animal per experiment. For survival experiments, animals were treated starting either 5 h before the infection (prophylactic regimen) or on day 1 or 2 after the infection (therapeutic regimens). In either case, PMO/P-PMO treatment was then further administered to the mice on a daily basis until the animals began to regain lost weight. The weight of each animal was recorded daily before drug injection.

**Tissue collection and histology.** Mice were euthanized with a solution of 2% (wt/vol) chloral hydrate in PBS and then perfused with 10 ml PBS to prevent possible contamination of organ samples by viruses circulating in the blood. Tissue samples taken from the same organ region of each animal were collected for histology studies or frozen at −80°C for subsequent virus titration. Frozen tissues were weighed and homogenized in 1.2 ml of Dulbecco's modified Eagle's medium by using a Mini-Bead-Beater (Biospec), and viral titers were determined by plaque assay. Samples collected for histology studies were preserved in 10% buffered formalin. Fixed tissues were embedded in paraffin, sectioned, and stained with hematoxylin and eosin (H&E). To quantify pathological changes in the livers, necrotic lesions were counted over an entire section chosen randomly for each animal. The area of each section was determined using a scanned image of the microscope slide and ImageJ software (NCBI). The upper limit of the number of lesions that could accurately be counted was estimated to be approximately 7 or 8 per $mm^2$. Individual lesions were not counted for sections that showed confluent necrosis.

## RESULTS

**Inhibition of translation in cell-free assay.** P-PMOs complementary to sequences in the MHV 5′-UTR (Table 1 and Fig. 1A) were evaluated in a translation inhibition assay. In vitro translation reactions were programmed with RNAs transcribed in vitro from a plasmid containing the entire 5′-UTR and the coding sequence for the first 14 amino acids of MHV-A59 pp1ab fused upstream of a luciferase reporter gene. Two P-PMOs binding near the 5′ terminus [5TERM and (+)18-39] and one complementary to the pp1ab AUG translation initiation region (AUG) were effective at submicromolar concentrations (Fig. 1B). Two P-PMOs complementary to the TRS region of the MHV leader (TRS1 and TRS2) were relatively

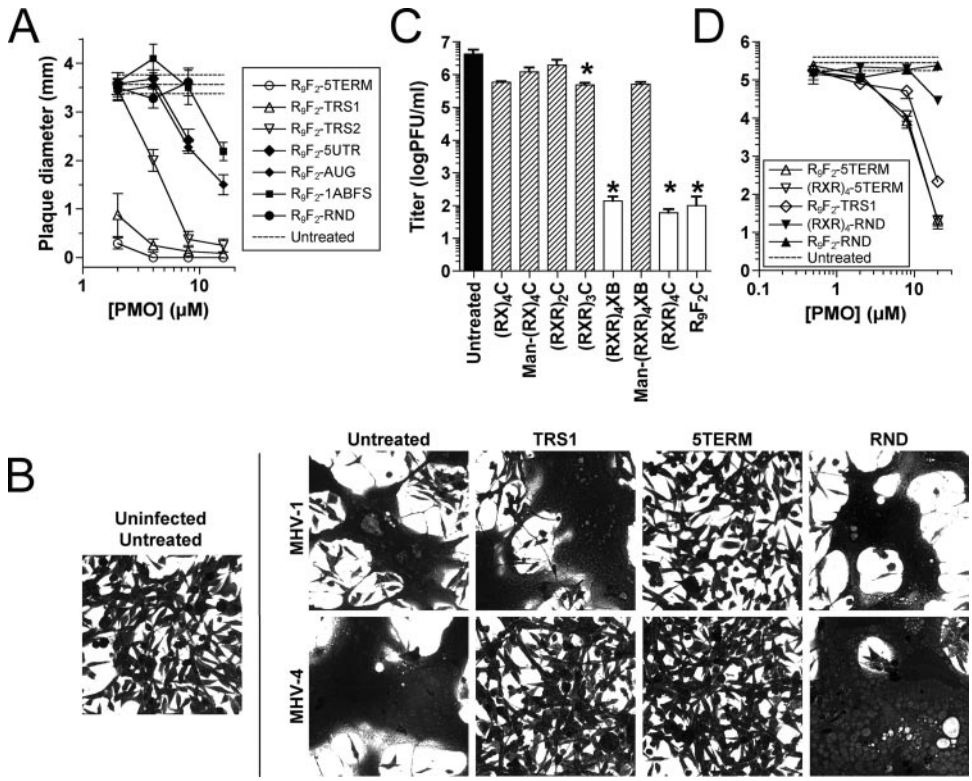


FIG. 2. Evaluation of PMO sequences and various peptide conjugates in MHV-infected cells. (A) Dose-dependent inhibition of MHV plaque expansion. DBT cell cultures were inoculated with fixed doses of MHV-A59, and an $R_9F_2$-PMO was added with each agarose overlay. The plaque diameter was then measured 72 h after the overlay was applied. (B) $R_9F_2$-PMO treatment reduces syncytium formation by MHV-1 and MHV-4. Qualitative changes in cell morphology and density were compared against untreated, uninfected (left) and untreated, infected (right [column marked untreated]) controls. Representative images show cells pretreated for 3 h with 10 μM $R_9F_2$-PMO and fixed for 24 h after inoculation. (C) Effects of delivery peptide conjugation on PMO activity. DBT cells were treated with 20 μM P-PMO for 3 h before inoculation at a multiplicity of 0.1 PFU/cell with MHV-A59. The virus yield was quantified 24 h after inoculation. 5′-Terminal peptide conjugates follow standard single-letter amino acid naming, except as follows: X, 6-aminohexanoic acid; B, beta-alanine; and Man, mannose. Asterisks indicate significant differences ($P < 0.05$ by Student's $t$ test) with respect to mock-treated controls. (D) Dose-response experiment comparing the effects of $R_9F_2$- and $(RXR)_4$-conjugated 5TERM, TRS1, and RND P-PMOs on viral titers. Cells were treated with various P-PMOs at 10 μM for 3 h, infected with MHV-A59 for 1 h, and then incubated again in the presence of P-PMOs for 24 h. Error bars throughout indicate standard errors of the means.

ineffective at reducing luciferase expression, whereas previous studies with analogous P-PMOs against wild-type SARS-CoV had suggested the TRS to be an excellent P-PMO target region (24).

**Inhibition of MHV in infected cells.** P-PMOs were tested for the following three correlates of antiviral activity in cell culture: reduction of viral cell-to-cell spread, cytopathology, and viral replication. $R_9F_2$-P-PMOs were added to the overlay of an MHV-A59 plaque assay to investigate effects on rate expansion from an infectious center (Fig. 2A). The P-PMO binding the viral 5′ terminus (5TERM) was most effective, followed closely by TRS-1. Other P-PMOs, targeting the 5′-UTR and the frameshift region (1ABFS), were moderately inhibitory. Two P-PMOs were completely ineffective in reducing cytopathology and spread from an infectious center [MBTRS and (−)3TERM], and two others [(+)18-39 and (−)18-39] appeared to generate inordinate cytotoxicity, as indicated by severe, concentration-dependent cell depletion over the course of a 3-day plaque size reduction assay relative to untreated and RND P-PMO-treated controls (data not shown). Ineffective and cytotoxic P-PMOs were excluded from further study.

$R_9F_2$-P-PMOs were next tested in DBT cells infected with MHV-1, MHV-2, MHV-3, MHV-4, and MHV-A59. Virus-induced cytopathic effects, including syncytium formation (MHV-1, MHV-3, MHV-4, and MHV-A59), rounding and detachment (MHV-2), and rapid cellular lysis (MHV-3), were reduced most consistently with the 5TERM P-PMO (Fig. 2B and data not shown). The TRS-1 P-PMO also provided an intermediate level of protection, likely through a mechanism other than direct inhibition of pp1ab translation (compare Fig. 1B and 2B).

**Peptide conjugate selection.** The most effective P-PMO sequence from the initial studies, 5TERM, was conjugated to several novel delivery peptides and tested for a reduction of release of infectious MHV-A59 from cells 24 h after inoculation (Fig. 2C). Two conjugates were the most effective, namely, the $R_9F_2$ peptide used above, which was previously employed for MHV and SARS-CoV antiviral studies (24, 25), and a peptide consisting of four repeats of arginine–6-amino-hexanoic acid (X)–arginine [$(RXR)_4$] followed by either a cysteine (C) or another single X residue and a beta-alanine (B) to serve as respective linkers (Fig. 2C). Further studies did not reveal differences in $(RXR)_4$-5TERM P-PMO effectiveness or toxicity related to linker composition, so the $(RXR)_4$XB conjugate,

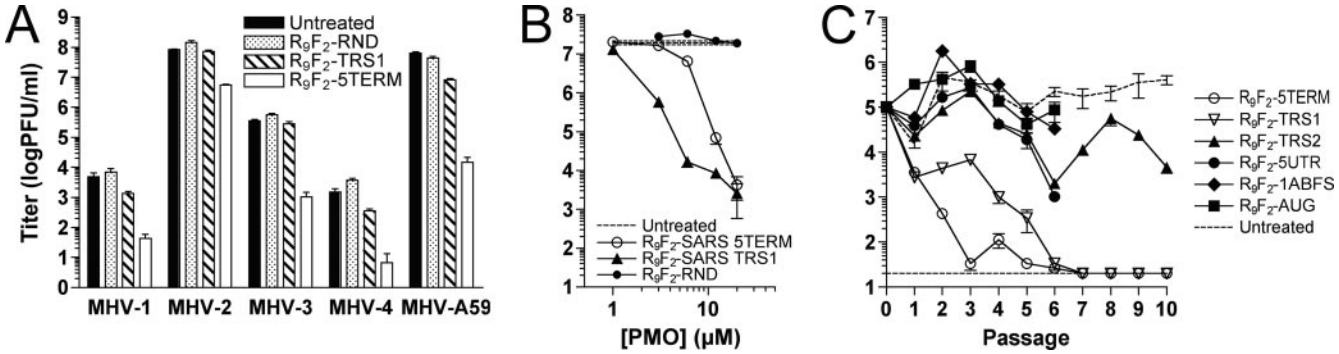


FIG. 3. Single-dose and long-term inhibition of coronavirus multiplication. (A) Inhibition of replication of various MHV strains (inoculated at multiplicities of 0.01 to 1 PFU/cell) in DBT cells after a 3-h preinoculation treatment with 10 μM P-PMO. The virus yield was quantified 24 h after inoculation. (B) Dose-activity comparison of the effects of SARS-5TERM and SARS-TRS1 P-PMOs on SARS-CoV (1 PFU/cell) in Vero-E6 cells. Cells were treated with P-PMOs for 6 h prior to inoculation, and viral titers were analyzed 48 h later. (C) Effects of long-term P-PMO treatment on MHV replication. DBT cells were treated for 6 h with P-PMOs and then inoculated with plaque-purified MHV-A59 (0.1 PFU/cell). Culture medium was used to inoculate fresh cultures of P-PMO-treated cells every 24 h for a total of 10 viral passages. The virus yield was quantified as described for panel A. Error bars throughout indicate standard errors of the means.

referred to hereafter simply as $(RXR)_4$, was selected for further experimentation due to the relative ease and efficiency of its synthesis. Conjugates with fewer arginine residues or with mannose modification were far less effective in this assay.

Dose efficacy determinations were performed with MHV-A59 for several of the most promising P-PMOs. The 5TERM PMO conjugated to $R_9F_2$ or $(RXR)_4$ was equally effective at reducing the viral titer. A randomized PMO (RND) conjugated to the $(RXR)_4$ peptide showed only mild nonspecific effects relative to the cognate $R_9F_2$-RND control conjugate (Fig. 2D). Therefore, both $R_9F_2$-5TERM and $(RXR)_4$-5TERM were selected for further testing in cell culture and in vivo.

**Broad-spectrum inhibition of MHV strains.** The relative effectiveness of $R_9F_2$-5TERM, $R_9F_2$-TRS1, and $R_9F_2$-RND was tested against a panel of MHV strains. Preinfection treatment of cells with $R_9F_2$-5TERM reduced titers of five MHV strains over 10-fold, with the strongest effects observed against MHV-A59 and MHV-3 (Fig. 3A). As in previous assays, $R_9F_2$-TRS1 treatment was less effective than $R_9F_2$-5TERM treatment at reducing viral titers, and $R_9F_2$-RND treatment slightly increased the release of infectious virus in several cases (Table 2).

These results showed that the 5TERM P-PMO was effective against several laboratory strains of MHV in cell culture. This multistrain inhibition was not surprising, since according to available sequence information, the MHV strains tested likely have perfect sequence identity at the 5TERM target site (data not shown). In order to determine whether the genomic 5′ terminus represents a highly effective P-PMO target site for coronaviruses in general, the corresponding challenge was carried out with SARS-CoV and a SARS-CoV-specific 5TERM P-PMO analog. However, dose-response testing revealed that a previously described P-PMO complementary to the SARS TRS region (SARS-TRS1) (24) was more effective than the SARS-5TERM P-PMO (Fig. 3B).

The effects of repetitive $R_9F_2$-PMO treatments on viral titer were also examined. Cell cultures were treated with those P-PMOs before inoculation with a freshly plaque-purified strain of MHV-A59. A 10 μM P-PMO concentration was selected for testing based on a similar published study with SARS-CoV (24). Serial treatment with the 5TERM or TRS1 P-PMO resulted in extinction of MHV-A59, while treatment with less effective P-PMOs did not strongly inhibit virus growth (Fig. 3C). While it is likely that sustained treatment with lower concentrations of the 5TERM $R_9F_2$-PMO would have eventually produced P-PMO-resistant virus, in a manner similar to that observed previously (24), this experiment demonstrated that repeated short-term treatments with an effective P-PMO can exert a cumulative effect on MHV replication.

**In vivo P-PMO dose determination.** For our experiments in vivo, we selected somewhat lower PMO and P-PMO dosing levels than those employed in other PMO/P-PMO in vivo studies (~20 to 33 mg of nonconjugated PMO/kg of body weight was reported in references 6 and 34, and 10 mg/kg P-PMO was reported in reference 38) in order to minimize the potential for

TABLE 2. Summary of P-PMO effectiveness

| P-PMO | $EC_{50}$ (nM)[a] | $IC_{50}$ (μM)[b] | Strain | Log decrease in titer[c] |
|---|---|---|---|---|
| $R_9F_2$-5TERM | 16 | 1.46 | MHV-1 | 2.05 |
| | | | MHV-2 | 1.19 |
| | | | MHV-3 | 2.45 |
| | | | MHV-4 | 2.35 |
| | | | MHV-A59 | 3.63 |
| $R_9F_2$-(+)18-39 | 51 | 1.42 | NT[d] | NT[d] |
| $R_9F_2$-TRS1 | >1,000 | 2.08 | MHV-1 | 0.55 |
| | | | MHV-2 | 0.05 |
| | | | MHV-3 | 0.11 |
| | | | MHV-4 | 0.63 |
| | | | MHV-A59 | 0.87 |
| $R_9F_2$-AUG | 335 | 2.73 | NT[d] | NT[d] |
| $R_9F_2$-RND | >1,000 | >20 | MHV-1 | −0.15 |
| | | | MHV-2 | −0.25 |
| | | | MHV-3 | −0.21 |
| | | | MHV-4 | −0.40 |
| | | | MHV-A59 | 0.16 |

[a] Concentration giving 50% reduction of luciferase expression in cell-free translation assays relative to that in untreated controls.
[b] Concentration giving 50% reduction of MHV-A59 titer at 24 h p.i. following 6 h of P-PMO pretreatment.
[c] Average $\log_{10}$ decrease in titer at 24 h p.i. following 6 h of pretreatment with 10 μM P-PMO relative to that for untreated control. Negative values describe elevated titers.
[d] NT, not tested.

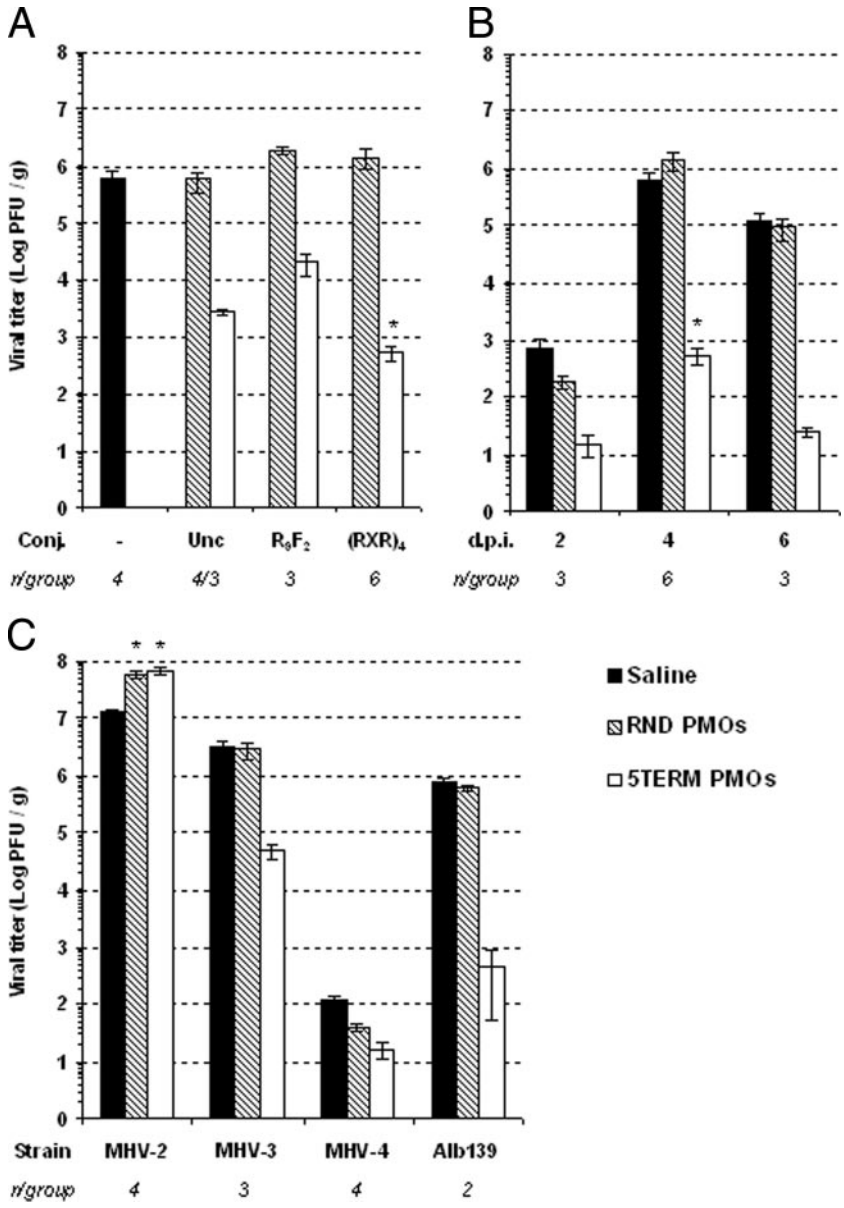


FIG. 4. 5TERM PMO and P-PMO reduce viral titers in the livers of MHV-infected mice. Mice were inoculated i.p. with MHV-A59 (A and B) or various other MHV strains (C). Starting 5 h before infection and on each of the next 2 days, each animal received one dose of saline (black bars), RND PMO or $(RXR)_4$-PMO (hatched bars), or 5TERM PMO or $(RXR)_4$-PMO (white bars), as indicated in Materials and Methods. $(RXR)_4$-PMO was utilized for panels B and C. Unc, unconjugated. Livers were collected on day 4 (A and C) or at the indicated time points (B), and viral titers were determined by plaque assay. Error bars indicate standard errors of the means. Asterisks indicate significant differences from mock-treated controls ($P < 0.05$ by Student's $t$ test).

side effects. To evaluate the toxicity of a particular dose for MHV PMOs and P-PMOs, mice were injected i.p. once per day for 4 days with 20 nanomoles of nonconjugated PMO or 8 nanomoles of P-PMO (equivalent to approximately 6.5 to 7.0 mg/kg PMO or 3.6 to 3.8 mg/kg P-PMO) in the absence of virus. P-PMO-treated and saline-injected control animals did not differ in appearance, behavior, or relative weight gain during or following treatment (data not shown). Moreover, H&E-stained liver sections obtained from these mice on the last day of the experiment did not exhibit any unusual features or apparent histopathology compared to those from saline-injected controls (see example included in Fig. 5C; data not shown). Based on these results, a dose of 20 nanomoles of nonconjugated PMO or 8 nanomoles of P-PMO was utilized throughout the remainder of the studies.

**Conjugate selection in vivo.** In order to select an appropriate measurement for in vivo antiviral activity, replication of MHV-A59 was evaluated in selected organs. Mice were inoculated i.p. with MHV-A59, and 4 days after the infection, blood was collected by cardiac puncture and samples were taken from the kidneys, intestines, and liver tissue. Viral titers were consistently near or below the limit of detection in kidney, intestine,

and blood samples, making it impossible to assess the potential antiviral activities of the P-PMOs in these organs (data not shown). Titers approached $10^6$ PFU per gram of liver tissue on day 4 p.i. (data not shown), and published studies with nonconjugated of morpholino oligomers had previously demonstrated high activity in the liver (29), and hence, a reduction of liver titer was chosen as the primary test for antiviral activity.

We next examined the effects of 5TERM PMO and P-PMO treatment on MHV replication in vivo. Initial in vivo testing of each delivery conjugate was limited to two mice per treatment group. Treatment with the $R_9F_2$-, $(RXR)_4XB$-, and $(RXR)_4C$-5TERM P-PMOs reduced MHV-A59 titers in the liver approximately 100-fold, but the other conjugations, including Man-$(RXR)_4XB$, reduced titers <10-fold compared to those of mock-treated controls (data not shown). These results were generally consistent with previous results from cell culture assays (Fig. 2C) and established the $(RXR)_4$ conjugates as the most effective. Additional experiments confirmed that treatment with nonconjugated, $R_9F_2$-, or $(RXR)_4$-5TERM PMO formulations reduced liver titers at least 100-fold relative to those of controls on day 4 p.i. (Fig. 4A). The $(RXR)_4$-5TERM treatment reduced liver titers at least 1,000-fold at the selected treatment dose and was therefore selected for subsequent i.p. challenge experiments.

**Reduction of viral load in livers infected with different MHV strains.** Livers were collected from P-PMO-treated mice 2, 4, and 6 days after inoculation with 1,000 PFU MHV-A59 and mock or P-PMO treatments on days 0, 1, and 2. The titers of $(RXR)_4$-5TERM-treated mice were strongly reduced compared to those of controls at all three time points assayed (Fig. 4B). Although treatment ceased on day 2 p.i., MHV titers remained strongly suppressed on day 6 p.i. (Fig. 4B). The effect of $(RXR)_4$-5TERM P-PMO treatment on replication of different strains of MHV was then examined. Mice were inoculated i.p. with 100 PFU of MHV-2, MHV-3 (20 50% lethal doses [$LD_{50}$]), or MHV-Alb139 ($5 \times 10^{-3}$ $LD_{50}$) and treated, as described above, with three doses of 5TERM P-PMO, RND P-PMO, or saline vehicle. Liver titers were determined at 4 days p.i. (Fig. 4C). The titers of Alb139, MHV-3, and MHV-4 were highly, moderately, and mildly reduced, respectively, compared to those of controls. Titers of MHV-2 were not reduced, in contrast to the effects of $R_9F_2$-5TERM P-PMO on this strain previously observed in cell culture (Fig. 3A). Conversely, a small but reproducible increase of the liver MHV-2 titer compared to that for the mock-treated controls was observed following 5TERM and RND P-PMO treatment (Fig. 4C). These results indicated that P-PMO treatment was effective against challenge with most, but not all, strains of MHV in vivo.

**Reduction of liver pathology.** H&E-stained liver sections from the mice used in the above experiments were examined to determine the effects of P-PMO treatment on histopathology in MHV-infected mice. Figure 5A shows a quantitative representation of the necrotic lesions in livers from mock-treated or P-PMO-treated, MHV-infected mice. Very few lesions were observed in the sections obtained from MHV-A59-infected control mice at 2 and 4 days p.i., thus making the absence of any lesions in the $(RXR)_4$-5TERM-treated mice at these time points inconclusive (data not shown). The frequency of lesions was significantly reduced on day 6 in $(RXR)_4$-5TERM-treated mice compared to that for controls (Fig. 5A, D, and E). $(RXR)_4$-5TERM treatment also reduced the numbers of lesions in animals infected with MHV-3, Alb139 (Fig. 5A), and MHV-4 (data not shown). The effects of P-PMO treatment were particularly striking in MHV-3-infected mice. The liver parenchyma from each of the six control animals displayed few recognizable hepatocytes (>90% of the section surface was necrotic in each sample), while livers from $(RXR)_4$-5TERM-treated mice showed small numbers of nonconfluent foci (Fig. 5F and G). In the case of MHV-2, although two of the four controls had too many lesions to allow quantitation, the other two controls displayed numbers similar to those for the $(RXR)_4$-5TERM-treated animals. Where necrotic lesions were present, the treatment with the 5TERM P-PMO resulted in no difference in the average diameter of individual lesions (data not shown), suggesting that the 5TERM P-PMO was most protective early in infection but was less effective in preventing the spread of an established infection foci. Overall, the levels of liver histopathology in the various groups were accurately predicted by the previous viral titer experiments (Fig. 4).

Liver sections from P-PMO- and mock-treated infected mice were examined for qualitative differences in the severity of hepatitis (Fig. 5H). The portal architecture was generally preserved in each infection model, but the type and degree of lymphocytic infiltration and necrosis in the parenchyma varied by MHV strain, as described in the literature (15). MHV-Alb139 and -A59-infected livers displayed lesions of ballooning necrosis with a marked lymphoid response, regardless of treatment (Fig. 5H). Livers from mock-treated and RND P-PMO-treated mice infected with MHV-3 displayed widespread coagulation necrosis with moderate inflammation. Treatment of MHV-3-infected mice with the 5TERM P-PMO produced smaller areas of necrosis, which were similar in appearance to those observed in Alb139-infected mice (Fig. 5H). Overall, no qualitative differences in the hepatic lesions were noted between the untreated, mock-treated, and RND P-PMO-treated groups.

**Effects of treatment on disease outcome.** The effects of P-PMO treatment on clinical MHV-induced hepatitis were examined. Continuous daily treatment failed to protect mice inoculated with 10 PFU of MHV-3. Indeed, $(RXR)_4$-5TERM PMO-treated mice typically outlived the controls by an average of only about 1 day, a delay that was modest but statistically significant (Fig. 6A). This result suggested that a reduction of viral titer was insufficient to prevent initiation of the coagulation cascade by MHV-3 (15).

Mice infected with up to 1,000 PFU MHV-A59 developed undetectable or modest clinical signs of disease. At this dose, a qualitative benefit of $(RXR)_4$-5TERM treatment was still observed, as the mice treated with the 5TERM P-PMO started to regain lost weight at day 5 p.i. after dropping to 96% of their initial weight, while mock- and RND P-PMO-treated mice continued to lose weight, down to 92% and 91%, respectively, on average, at day 7 p.i. (data not shown). Similar results, i.e., a faster recovery of 5TERM P-PMO-treated mice, were also obtained after infection with 100 PFU (Fig. 6B) or 1,000 PFU (data not shown) Alb139. When mice were injected with 10,000 PFU Alb139, a clear beneficial effect of the prophylactic treatment with $(RXR)_4$-5TERM was also observed (Fig. 6C). Indeed, the average weight loss was limited to 7% for the

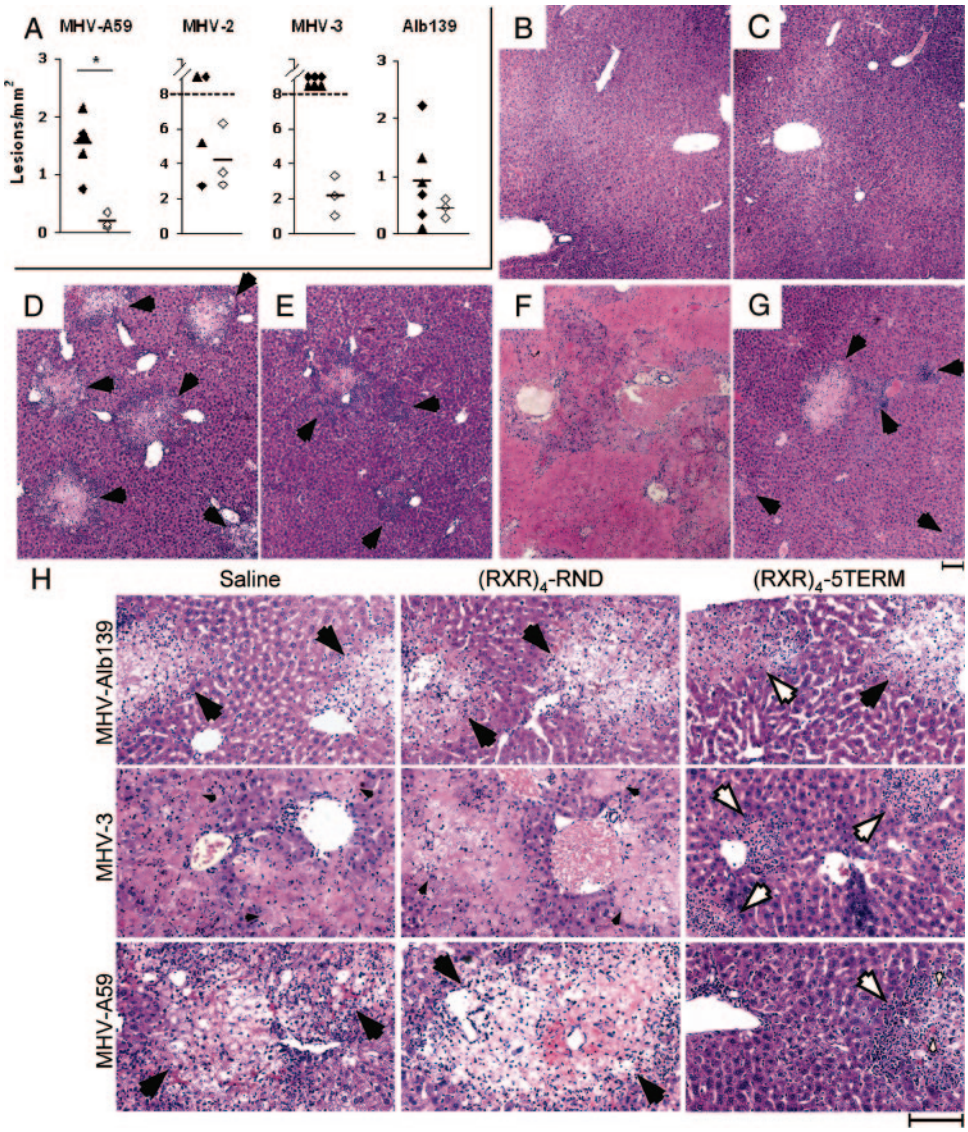


FIG. 5. 5TERM-$(RXR)_4$-PMO attenuates viral hepatitis. (A) Livers were obtained from mice infected with the indicated MHV strains at 4 (MHV-2, MHV-3, and MHV-Alb139) or 6 (MHV-A59) days p.i. The numbers of necrotic lesions per unit area were compared between P-PMO-treated and mock-treated groups, as described in Materials and Methods. Data points represent individual mice, and bars indicate the mean severities for the combined mock- and RND P-PMO-treated groups and the 5TERM P-PMO-treated group, respectively. The number of lesions was significantly lower in A59-infected mice treated with 5TERM P-PMO than in mock-treated ($P < 0.05$) or RND P-PMO-treated ($P < 0.005$) controls. (B to G) Representative areas of H&E-stained livers from uninfected (B and C) and MHV-A59 (D and E [6 days p.i.])- and MHV-3 (F and G [4 days p.i.])-infected animals. Mice received $(RXR)_4$-5TERM P-PMO treatment (C, E, and G) or mock treatment (B, D, and F). Necrotic lesions and inflammation characteristic of lymphocytes are indicated with arrowheads. Note the regions of bright pink staining that mark necrotic areas in panel E. (H) At a higher magnification, the liver sections show ballooning necrosis (large black arrowheads), lymphocytic infiltration with more moderate necrosis (large white arrowheads), widespread coagulation necrosis with karyorrhectic debris (small black arrowheads), and eosinophilic staining reminiscent of Councilman bodies (small white arrowheads). Bars, 0.1 mm.

5TERM P-PMO-treated mice, while the average weight of mock-treated controls decreased up to 18% (Fig. 6C). All mice treated with $(RXR)_4$-5TERM before inoculation and all mice in the mock-treated control group survived the experiment. Notably, when $(RXR)_4$-5TERM treatment was delayed until the first day after the infection, the mice lost weight more rapidly than the controls, and eventually all succumbed between days 5 and 8 p.i. (Fig. 6C). Similarly, mice that had received the RND P-PMO lost weight more rapidly than the mock-treated animals, and two of three died on day 5, while the last one survived the experiment (Fig. 6C).

At a fivefold higher dose of Alb139, which proved to be lethal in all mock-treated controls between days 5 and 7 p.i., the prophylactic treatment with $(RXR)_4$-5TERM increased survival by only one additional day, on average (Fig. 6D). Again, mice treated with $(RXR)_4$-RND lost weight significantly more rapidly than did mock-treated controls, and all died by day 6 p.i. (Fig. 6D). To summarize, these experiments

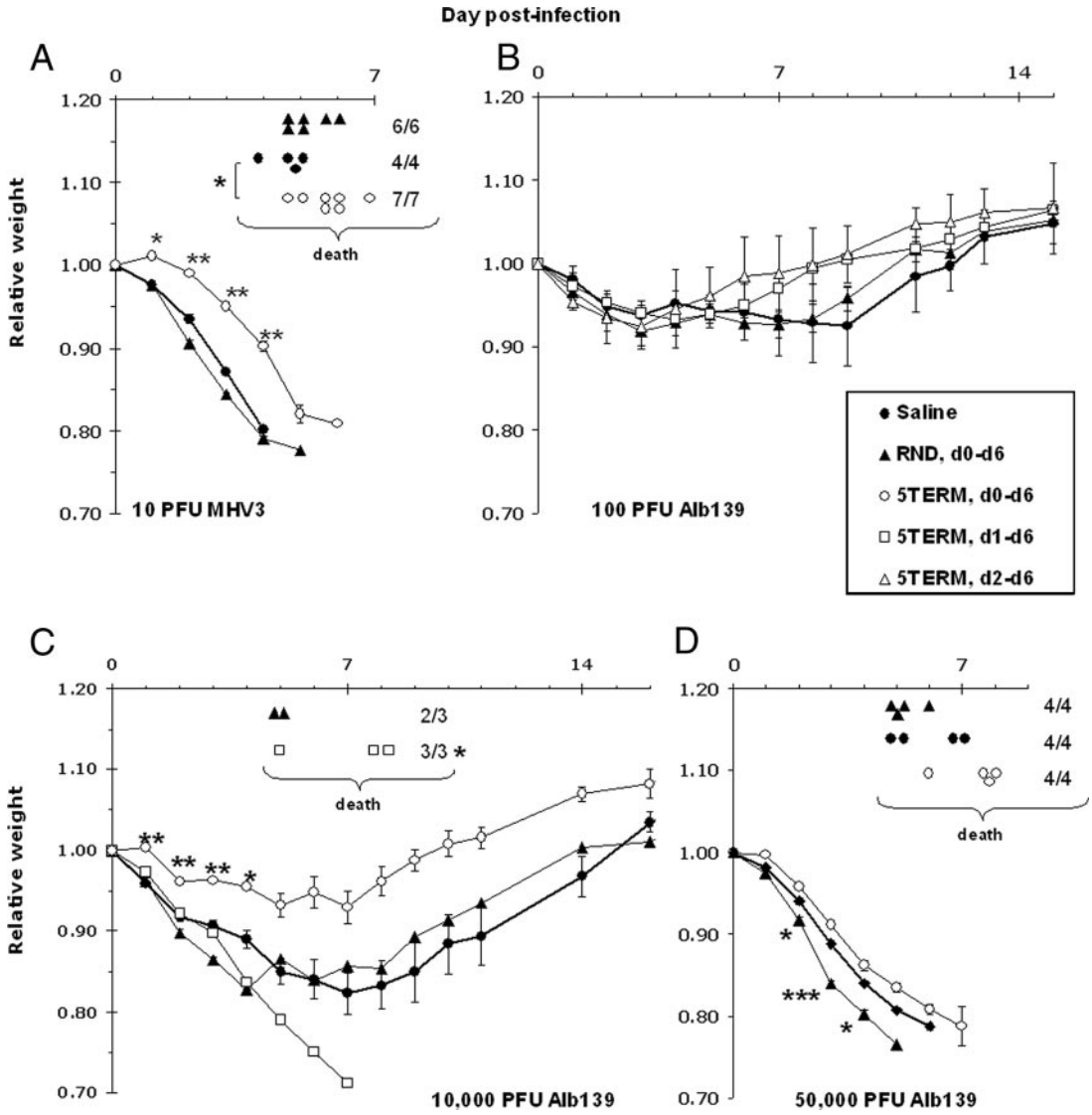


FIG. 6. Dual effects of $(RXR)_4$-5TERM on weight loss and survival. Mice were infected with 10 PFU MHV-3 (A) or 100 (B), 10,000 (C), or 50,000 (D) PFU MHV-Alb139. Depending on the experiment, some animals received $(RXR)_4$-5TERM, following either a prophylactic (empty circles) or therapeutic (empty squares and empty triangles) regimen. Controls received either saline (black circles) or $(RXR)_4$-RND (black triangles) daily, with the first injection starting 5 h before inoculation. The relative weight is shown for each treatment group ($n = 3$ to 7). Error bars indicate standard errors of the means. Each death is represented with the group's corresponding symbol positioned on the time axis at the time of the event. Asterisks indicate significant differences relative to the mock-treated control group. *, $P < 0.05$; **, $P < 0.01$. Student's $t$ test (weight) or the log rank survival test (mortality) was used to determine statistical significance.

showed that treatment with the 5TERM P-PMO displayed a beneficial effect when the inoculum dose was relatively low or when the drug was administered before infection in those cases where a relatively high dose of virus was used. In the latter experiments, delayed treatment with the antiviral P-PMO or administration of a nonspecific P-PMO adversely affected the outcome of clinical disease (Fig. 6C and D).

**Effects of treatment on respiratory MHV infection.** We then evaluated the potential of PMOs in the treatment of coronavirus infection in the central nervous system. Mice were treated i.p. with a PMO or $(RXR)_4$-PMO 5 h before, 24 h after, and 48 h after intracranial inoculation with 10 PFU (0.1 $LD_{50}$) MHV-A59. The average virus load per gram of brain tissue on day 4 p.i. was not affected by PMO or P-PMO treatment (data not shown). This result indicates that the amount of PMO or P-PMO delivered to the central nervous system after i.p. treatment was insufficient to exert a detectable antiviral effect, in accordance with the literature (29), and no further experiments were performed with this model.

To evaluate the potential of P-PMOs in the treatment of coronavirus infection of the respiratory system, we infected A/J mice i.n. with 100 PFU MHV-1, a dose that was selected to produce a severe but nonlethal disease, and treated them with a P-PMO or vehicle administered either i.n. or by i.p. injection. As shown in Fig. 7A, lung viral titers in animals treated prophylactically with $(RXR)_4$-5TERM administered i.n. were re-

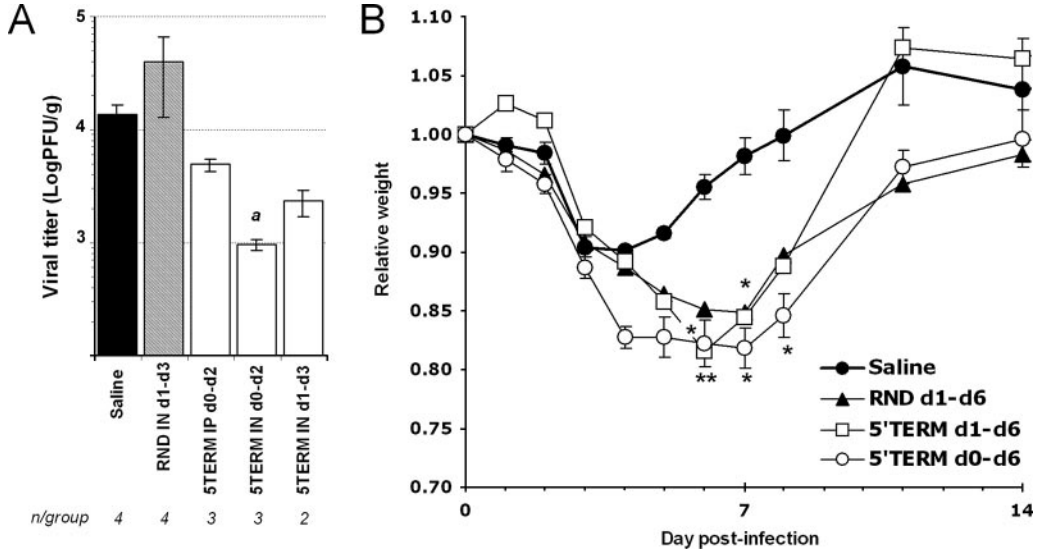


FIG. 7. P-PMOs in the lungs of MHV-1-infected mice. (A) Comparison of viral titers from lung homogenates collected 4 days after inoculation. As indicated, the treated groups received three doses of 5TERM $(RXR)_4$-PMO i.n. or i.p. starting 5 h before or 24 h after i.n. inoculation with 100 PFU MHV-1. The designation "a" marks a nonsignificant trend of difference from mock-treated controls ($P = 0.057$ by Student's $t$ test). (B) Clinical disease in A/J mice infected with 50 PFU MHV-1 and treated i.n. as indicated. Daily weight values are expressed as a percentage of the initial weight of each animal. Error bars indicate the standard error of the mean for each group ($n = 4$/group, except for the RND P-PMO group [$n = 1$]). Asterisks indicate significant differences relative to the mock-treated control group. *, $P < 0.05$; **, $P < 0.01$ (Student's $t$ test).

duced over 10-fold compared to those of controls, while corresponding i.p. treatment resulted in only a 2-fold decrease of viral titer. Mice treated with $(RXR)_4$-5TERM i.n. starting on day 1 p.i. displayed a fivefold reduction of viral titer (Fig. 7A). Examination of the lung histopathology on day 4 p.i. showed mild focal inflammation and edema in most of the animals but did not reveal any consistent difference between the antisense PMO-treated and control groups (data not shown).

Finally, the effects of P-PMO treatment on the clinical health of the mice in the respiratory model were examined. As shown in Fig. 7B, mice in both P-PMO-treated groups continued to lose weight from days 4 to 6 p.i., while the mock-treated controls started to regain lost weight at this stage. All mice eventually recovered from the infection in this experiment. Thus, although antiviral effects of P-PMO treatment were observed in the MHV-1 respiratory disease model, P-PMO treatment also apparently resulted in an exacerbation of clinical disease.

## DISCUSSION

This study documents that a P-PMO (5TERM) designed to duplex with the 5′-terminal sequence of the MHV genome was able to inhibit viral replication both in cell culture and in vivo. The 5TERM P-PMO had antiviral efficacy against six strains of MHV in cell culture and was active against five of those strains in mice. In contrast to a previous study (24), preliminary screening of various P-PMOs in a cell-free translation assay did not accurately predict the relative efficacies of those P-PMOs against whole viruses in cell culture. The TRS1 P-PMO, which was only marginally active in cell-free translation inhibition assays, was relatively potent in antiviral assays (Table 2). These data also suggest that various levels of interference with viral RNA synthesis, rather than inhibition of replicase translation, may differentiate the activities of various P-PMOs with partially overlapping target sequences in the leader TRS region.

The 72-nt leader regions of MHV and SARS-CoV have low sequence identity (32%), although the leader TRS sequence of each virus is positioned similarly, at positions 66 to 72 for MHV and 67 to 72 for SARS-CoV. In cell culture assays, MHV-TRS1 (target nt 51 to 72) and SARS-TRS2 (target nt 56 to 76) (24) were considerably more active than MHV-TRS2 (target nt 60 to 82) and SARS-TRS1 (target nt 53 to 72), respectively. Further experimentation will be required to determine where viral enzymes, such as the Nsp15 uridylate-specific endonuclease (3), footprint on replicative-form RNA during the discontinuous phase of coronavirus negative-strand RNA synthesis (28). Such studies may provide a rational explanation for the differential activity of P-PMOs complementary to various locations in the TRS region.

A P-PMO complementary to the 5′-terminal region of MHV genomic RNA produced the most robust activity against MHV. However, a P-PMO complementary to the TRS region of SARS-CoV displayed higher antiviral activity than the SARS-CoV 5TERM P-PMO in cell culture experiments with wild-type virus (Fig. 3B). Thus, while the available data were sufficient to infer that the 5′ terminus and TRS region contain P-PMO targets with high potential for antiviral activity, preliminary screening of P-PMOs against live viruses in cell culture appears to be necessary for accurate evaluation of efficacy and for the selection of candidates for in vivo testing.

The composition of the delivery peptide conjugated to the 5TERM PMO was a critical determinant of antiviral activity in cell culture and in vivo. Generally, conjugates with eight or nine arginines outperformed conjugates with fewer arginines in cell culture assays (Fig. 2C), consistent with an earlier report (21). Despite the apparent equivalency of the $R_9F_2$ and

$(RXR)_4$ peptide conjugates in cell culture (Fig. 2D), $(RXR)_4$ conjugates were more active in mice (Fig. 4A). The greater activity of $(RXR)_4$ conjugates may be due to their higher metabolic stability in circulation (37) and lesser trapping in endosomes/lysosomes (2) than those of the $R_9F_2$ conjugate. These results suggest that insertion of 6-aminohexanoic acid within polyarginine or polybasic tracts may confer greater potency to a P-PMO through enhanced stability and/or intracellular behavior, although further experimentation will be required to determine the mechanism resulting in superior activity. In contrast to reports that showed enhanced liver uptake of PNA and TFO through their conjugation to carbohydrates (10, 36), mannose modification reduced the activity of $(RXR)_4$-5TERM significantly both in cell culture and in vivo. In addition, mannose modification of the $(RX)_4$-5TERM conjugate did not enhance its activity (data not shown). We can offer several plausible explanations for these observations. The bulkiness of three mannose-modified serine residues may have inhibited the delivery of these compounds into cells by interfering with the P-PMO association with cell surface proteoglycans important for cellular uptake of an $(RXR)_4$-PMO conjugate (2). Similarly, the P-PMO portion of the mannosylated P-PMO may interfere with the binding of mannose to cognate receptors. It is also possible that the mannose moiety may enhance the uptake of P-PMOs preferentially into cell types insignificant to viral pathology. It is noteworthy that although nonconjugated PMOs generated substantial antiviral activity in vivo, $(RXR)_4$-PMOs were approximately 10 times as effective at approximately half the concentration (Fig. 4A).

5TERM P-PMO treatment reduced MHV titers in the liver. When using MHV-A59, we found that administration of three doses of 5TERM P-PMO early in infection resulted in long-lasting suppression of viral replication. Similar observations were reported for recent studies with PMO compounds specific to Ebola virus (34) and coxsackievirus B3 (38). $(RXR)_4$-5TERM was active against all the strains tested in mice, except for MHV-2. On the contrary, liver titers in MHV-2-infected animals treated with either the control or virus-specific P-PMO were significantly higher than those in mock-treated controls. MHV-2 is the strain that replicated to the highest titers in the liver, and rapid replication and a high viral load in this organ could explain the discrepancy with the data obtained in cell culture, where 5TERM P-PMO was nearly as effective against MHV-2 as against the other MHV strains. Despite repeated attempts, we were unable to sequence the 5′-terminal region of the genomic RNA of the MHV-2 isolate used in this study. However, the 5TERM PMO binding site was absolutely conserved among the other strains of MHV for which sequence information was available, and therefore sequence variance is unlikely to account for the discrepancy between the results of cell culture and animal experiments.

MHV-3-infected mice succumb to fulminant hepatitis, where cellular damage is provoked not only by the virus but also through activation of the coagulation cascade in response to infection (15). Treatment with dmPGE2, a prostaglandin analog, has been reported to reduce liver damage in MHV-3-susceptible mice, despite negligible effects on the level of viral replication (1). However, in previous studies, both the dmPGE2-treated mice and the controls died on day 5 (1). In a separate report, ribavirin treatment during MHV-3 infection prolonged survival, but again only to day 5 (16). Likewise, in our experiments, reduced viral titers were found to result in a reduction of liver necrosis, yet the lethal outcome was only slightly delayed.

MHV-A59 has been reported to provoke fatal murine hepatitis. Our laboratory-adapted MHV-A59 isolate displayed lower pathogenicity in vivo than that of a wild-type clone of A59, MHV-Alb139 (5). It has been reported that mutations in the sequence coding for the spike protein, resulting from in vitro adaptation to growth in glial cells, may result in attenuation in the liver (22), and this may constitute an explanation for the attenuated phenotype of our isolate of MHV-A59. Experiments to characterize mutations involved in the further attenuation of MHV-A59 are ongoing and will be reported elsewhere. We thus used Alb139 to obtain a more virulent, though not fulminant, hepatitis. Treatment with the 5TERM P-PMO limited the weight loss of mice that had received prophylactic treatment and inoculation of up to $10^4$ PFU of the virus. However, a noticeable exacerbation of the clinical disease was observed both for the group where treatment with the 5TERM P-PMO was delayed until day 1 after inoculation and for the group that received the RND P-PMO with the highest doses of Alb139. Likewise, despite a positive antiviral effect of P-PMOs observed in the lungs of MHV-1-infected mice, their clinical status was found to be slightly worsened in all the P-PMO-treated groups compared to that of the mock-treated controls.

Since a small increase of the viral titer in the presence of the RND-PMO was observed in experiments in vitro (Table 2) and in vivo (Fig. 4A and C [MHV-2] and 6C and D) and because an exacerbation of clinical disease was observed in both delayed 5TERM-PMO treatment groups (Fig. 6C and 7B), we hypothesized that P-PMOs, irrespective of sequence, may have a nonspecific enhancing effect on viral replication. This effect could not have been detected after treatment with effective doses of antiviral P-PMO and would only become noticeable when the sequence of the PMO was devoid of antiviral activity or when the MHV titer was too high to be contained by the treatment. To test this hypothesis, mice were inoculated with increasing doses of Alb139 (10, 100, 1,000, or 10,000 PFU) and received $(RXR)_4$-5TERM P-PMO or saline vehicle starting on day 1. While the drug was still able to decrease the viral titer 10-fold for the lowest dose of virus at 4 days p.i., we were unable to detect any significant difference between the viral loads in the livers of the two groups of animals at the three highest doses compared to untreated controls (data not shown) ($n = 3$ or 4/group). Thus, ineffective P-PMO treatment did not detectably enhance the levels of viral replication under these conditions. We are currently investigating how the choice of delivery peptide and PMO sequence affects disease augmentation. To determine if the exacerbated disease is specific to the coronaviruses, we are also examining the effects of control and antiviral P-PMOs in infection models using viruses from other families.

In summary, treatment with anti-coronaviral P-PMOs reduced viral titers both in vitro and in vivo. However, some treatment-related toxicity was evident under conditions where high loads of virus were present in the infected organs. These limitations may preclude wider therapeutic use of $(RXR)_4$-PMOs. The available data suggest that $(RXR)_4$-PMO may

still prove useful as prophylactic treatment for coronaviruses or if used as part of a combined antiviral therapy.

## ACKNOWLEDGMENTS

We thank the Chemistry Group at AVI Biopharma for expert production of all PMO compounds, Radin Aur, Andrew Kroeker, and Michelle Nelson for technical assistance, and Howard S. Fox for histopathology advice.

These studies were supported by NIH grants AI25913 and AI059799 to M.J.B. and by NIH-NIAID contract HHSN 266200400058C (Functional and Structural Proteomics of SARS-CoV).

This is TSRI manuscript no. 18467.

## REFERENCES

1. **Abecassis, M., J. A. Falk, L. Makowka, V. J. Dindzans, R. E. Falk, and G. A. Levy.** 1987. 16,16-Dimethyl prostaglandin E2 prevents the development of fulminant hepatitis and blocks the induction of monocyte/macrophage procoagulant activity after murine hepatitis virus strain 3 infection. J. Clin. Investig. **80:**881–889.
2. **Abes, S., H. M. Moulton, P. Clair, P. Prevot, D. S. Youngblood, R. P. Wu, P. L. Iversen, and B. Lebleu.** 2006. Vectorization of morpholino oligomers by the (R-Ahx-R)4 peptide allows efficient splicing correction in the absence of endosomolytic agents. J. Control. Release **116:**304–313.
3. **Bhardwaj, K., J. Sun, A. Holzenburg, L. A. Guarino, and C. C. Kao.** 2006. RNA recognition and cleavage by the SARS coronavirus endoribonuclease. J. Mol. Biol. **361:**243–256.
4. **Deas, T. S., I. Binduga-Gajewska, M. Tilgner, P. Ren, D. A. Stein, H. M. Moulton, P. L. Iversen, E. B. Kauffman, L. D. Kramer, and P. Y. Shi.** 2005. Inhibition of flavivirus infections by antisense oligomers specifically suppressing viral translation and RNA replication. J. Virol. **79:**4599–4609.
5. **de Haan, C. A., M. de Wit, L. Kuo, C. Montalto-Morrison, B. L. Haagmans, S. R. Weiss, P. S. Masters, and P. J. Rottier.** 2003. The glycosylation status of the murine hepatitis coronavirus M protein affects the interferogenic capacity of the virus in vitro and its ability to replicate in the liver but not the brain. Virology **312:**395–406.
6. **Enterlein, S., K. L. Warfield, D. L. Swenson, D. A. Stein, J. L. Smith, C. S. Gamble, A. D. Kroeker, P. L. Iversen, S. Bavari, and E. Mühlberger.** 2006. VP35 knockdown inhibits Ebola virus amplification and protects against lethal infection in mice. Antimicrob. Agents Chemother. **50:**984–993.
7. **Ge, Q., M. Pastey, D. Kobasa, P. Puthavathana, C. Lupfer, R. K. Bestwick, P. L. Iversen, J. Chen, and D. A. Stein.** 2006. Inhibition of multiple subtypes of influenza A virus in cell cultures with morpholino oligomers. Antimicrob. Agents Chemother. **50:**3724–3733.
8. **Gorbalenya, A. E., E. J. Snijder, and W. J. Spaan.** 2004. Severe acute respiratory syndrome coronavirus phylogeny: toward consensus. J. Virol. **78:**7863–7866.
9. **Guan, Y., B. J. Zheng, Y. Q. He, X. L. Liu, Z. X. Zhuang, C. L. Cheung, S. W. Luo, P. H. Li, L. J. Zhang, Y. J. Guan, K. M. Butt, K. L. Wong, K. W. Chan, W. Lim, K. F. Shortridge, K. Y. Yuen, J. S. Peiris, and L. L. Poon.** 2003. Isolation and characterization of viruses related to the SARS coronavirus from animals in southern China. Science **302:**276–278.
10. **Hamzavi, R., F. Dolle, B. Tavitian, O. Dahl, and P. E. Nielsen.** 2003. Modulation of the pharmacokinetic properties of PNA: preparation of galactosyl, mannosyl, fucosyl, *N*-acetylgalactosaminyl, and *N*-acetylglucosaminyl derivatives of aminoethylglycine peptide nucleic acid monomers and their incorporation into PNA oligomers. Bioconjug. Chem. **14:**941–954.
11. **Heasman, J.** 2002. Morpholino oligos: making sense of antisense? Dev. Biol. **243:**209–214.
12. **Holden, K. L., D. A. Stein, A. A. Pierson, K. Ahmed, P. Clyde, P. L. Iversen, and E. Harris.** 2006. Inhibition of dengue virus translation and RNA synthesis by a morpholino oligomer targeted to the top of the terminal 3′ stem-loop structure. Virology **344:**439–452.
13. **Kinney, R. M., C. Y. Huang, B. C. Rose, A. D. Kroeker, T. W. Dreher, P. L. Iversen, and D. A. Stein.** 2005. Inhibition of dengue virus serotypes 1 to 4 in Vero cell cultures with morpholino oligomers. J. Virol. **79:**5116–5128.
14. **Lane, T. E., and M. J. Buchmeier.** 1997. Murine coronavirus infection: a paradigm for virus-induced demyelinating disease. Trends Microbiol. **5:**9–14.
15. **Levy, G., and M. Abecassis.** 1989. Activation of the immune coagulation system by murine hepatitis virus strain 3. Rev. Infect. Dis. **11**(Suppl. 4)**:**S712–S721.
16. **Levy, G. A., G. Adamson, M. J. Phillips, L. A. Scrocchi, L. Fung, P. Biessels, N. F. Ng, A. Ghanekar, A. Rowe, M. X. Ma, A. Levy, C. Koscik, W. He, R. Gorczynski, S. Brookes, C. Woods, I. D. McGilvray, and D. Bell.** 2006. Targeted delivery of ribavirin improves outcome of murine viral fulminant hepatitis via enhanced anti-viral activity. Hepatology **43:**581–591.
17. **Li, W., Z. Shi, M. Yu, W. Ren, C. Smith, J. H. Epstein, H. Wang, G. Crameri, Z. Hu, H. Zhang, J. Zhang, J. McEachern, H. Field, P. Daszak, B. T. Eaton, S. Zhang, and L. F. Wang.** 2005. Bats are natural reservoirs of SARS-like coronaviruses. Science **310:**676–679.
18. **Liang, G., Q. Chen, J. Xu, Y. Liu, W. Lim, J. S. Peiris, L. J. Anderson, L. Ruan, H. Li, B. Kan, B. Di, P. Cheng, K. H. Chan, D. D. Erdman, S. Gu, X. Yan, W. Liang, D. Zhou, L. Haynes, S. Duan, X. Zhang, H. Zheng, Y. Gao, S. Tong, D. Li, L. Fang, P. Qin, and W. Xu.** 2004. Laboratory diagnosis of four recent sporadic cases of community-acquired SARS, Guangdong Province, China. Emerg. Infect. Dis. **10:**1774–1781.
19. **Masters, P. S.** 1999. Reverse genetics of the largest RNA viruses. Adv. Virus Res. **53:**245–264.
20. **Moulton, H. M., M. C. Hase, K. M. Smith, and P. L. Iversen.** 2003. HIV Tat peptide enhances cellular delivery of antisense morpholino oligomers. Antisense Nucleic Acid Drug Dev. **13:**31–43.
21. **Moulton, H. M., M. H. Nelson, S. A. Hatlevig, M. T. Reddy, and P. L. Iversen.** 2004. Cellular uptake of antisense morpholino oligomers conjugated to arginine-rich peptides. Bioconjug. Chem. **15:**290–299.
22. **Navas-Martin, S., S. T. Hingley, and S. R. Weiss.** 2005. Murine coronavirus evolution in vivo: functional compensation of a detrimental amino acid substitution in the receptor binding domain of the spike glycoprotein. J. Virol. **79:**7629–7640.
23. **Nelson, M. H., D. A. Stein, A. D. Kroeker, S. A. Hatlevig, P. L. Iversen, and H. M. Moulton.** 2005. Arginine-rich peptide conjugation to morpholino oligomers: effects on antisense activity and specificity. Bioconjug. Chem. **16:**959–966.
24. **Neuman, B. W., D. A. Stein, A. D. Kroeker, M. J. Churchill, A. M. Kim, P. Kuhn, P. Dawson, H. M. Moulton, R. K. Bestwick, P. L. Iversen, and M. J. Buchmeier.** 2005. Inhibition, escape, and attenuated growth of severe acute respiratory syndrome coronavirus treated with antisense morpholino oligomers. J. Virol. **79:**9665–9676.
25. **Neuman, B. W., D. A. Stein, A. D. Kroeker, A. D. Paulino, H. M. Moulton, P. L. Iversen, and M. J. Buchmeier.** 2004. Antisense morpholino-oligomers directed against the 5′ end of the genome inhibit coronavirus proliferation and growth. J. Virol. **78:**5891–5899.
26. **Normile, D.** 2004. Infectious diseases. Mounting lab accidents raise SARS fears. Science **304:**659–661.
27. **Parker, S. E., T. M. Gallagher, and M. J. Buchmeier.** 1989. Sequence analysis reveals extensive polymorphism and evidence of deletions within the E2 glycoprotein gene of several strains of murine hepatitis virus. Virology **173:** 664–673.
28. **Pasternak, A. O., W. J. Spaan, and E. J. Snijder.** 2006. Nidovirus transcription: how to make sense. . .? J. Gen. Virol. **87:**1403–1421.
29. **Sazani, P., F. Gemignani, S. H. Kang, M. A. Maier, M. Manoharan, M. Persmark, D. Bortner, and R. Kole.** 2002. Systemically delivered antisense oligomers upregulate gene expression in mouse tissues. Nat. Biotechnol. **20:**1228–1233.
30. **Summerton, J., and D. Weller.** 1997. Morpholino antisense oligomers: design, preparation, and properties. Antisense Nucleic Acid Drug Dev. **7:**187–195.
31. **Summerton, J. J.** 1999. Morpholino antisense oligomers: the case for an RNase H-independent structural type. Biochim. Biophys. Acta **1489:**141–158.
32. **van den Born, E., D. A. Stein, P. L. Iversen, and E. J. Snijder.** 2005. Antiviral activity of morpholino oligomers designed to block various aspects of equine arteritis virus amplification in cell culture. J. Gen. Virol. **86:**3081–3090.
33. **van der Hoek, L., K. Pyrc, M. F. Jebbink, W. Vermeulen-Oost, R. J. Berkhout, K. C. Wolthers, P. M. Wertheim-van Dillen, J. Kaandorp, J. Spaargaren, and B. Berkhout.** 2004. Identification of a new human coronavirus. Nat. Med. **10:**368–373.
34. **Warfield, K. L., D. L. Swenson, G. G. Olinger, D. K. Nichols, W. D. Pratt, R. Blouch, D. A. Stein, M. J. Aman, P. L. Iversen, and S. Bavari.** 2006. Gene-specific countermeasures against Ebola virus based on antisense phosphorodiamidate morpholino oligomers. PLoS Pathog. **2:**e1.
35. **Woo, P. C., S. K. Lau, C. M. Chu, K. H. Chan, H. W. Tsoi, Y. Huang, B. H. Wong, R. W. Poon, J. J. Cai, W. K. Luk, L. L. Poon, S. S. Wong, Y. Guan, J. S. Peiris, and K. Y. Yuen.** 2005. Characterization and complete genome sequence of a novel coronavirus, coronavirus HKU1, from patients with pneumonia. J. Virol. **79:**884–895.
36. **Ye, Z., K. Cheng, R. V. Guntaka, and R. I. Mahato.** 2005. Targeted delivery of a triplex-forming oligonucleotide to hepatic stellate cells. Biochemistry **44:**4466–4476.
37. **Youngblood, D. S., S. A. Hatlevig, J. N. Hassinger, P. L. Iversen, and H. M. Moulton.** 2007. Stability of cell-penetrating peptide-morpholino oligomer conjugates in human serum and in cells. Bioconjug. Chem. **18:**50–60.
38. **Yuan, J., D. A. Stein, T. Lim, D. Qiu, S. Coughlin, Z. Liu, Y. Wang, R. Bouch, H. M. Moulton, P. L. Iversen, and D. Yang.** 2006. Inhibition of coxsackievirus B3 in cell cultures and in mice by peptide-conjugated morpholino oligomers targeting the internal ribosome entry site. J. Virol. **80:**11510–11519.
39. **Zhang, Y. J., D. A. Stein, S. M. Fan, K. Y. Wang, A. D. Kroeker, X. J. Meng, P. L. Iversen, and D. O. Matson.** 2006. Suppression of porcine reproductive and respiratory syndrome virus replication by morpholino antisense oligomers. Vet. Microbiol. **117:**117–129.
40. **Zorzitto, J., C. L. Galligan, J. J. Ueng, and E. N. Fish.** 2006. Characterization of the antiviral effects of interferon-alpha against a SARS-like coronavirus infection in vitro. Cell Res. **16:**220–229.